Modelling and Coordinated Control of Grid Connected Photovoltaic, Wind Turbine Driven PMSG, and Energy Storage Device for a Hybrid DC/AC Microgrid

Prabhakaran Koothu Kesavan, *Senior Member*, *IEEE*, Umashankar Subramaniam, *Senior Member*, *IEEE*, Dhafer Jaber Almakhles, *Senior Member*, *IEEE*, and Sivakumar Selvam, *Senior Member*, *IEEE*

***Abstract*—In a DC/AC microgrid system, the issues of DC bus voltage regulation and power sharing have been the subject of a significant amount of research. Integration of renewable energy into the grid involves multiple converters and these are vulnerable to perturbations caused by transient events. To enhance the flexibility and controllability of the grid connected converter (GCC), this paper proposes a common DC bus voltage maintenance and power sharing control strategy of a GCC for a DC/AC microgrid. A maximum power point tracking algorithm is employed to enhance the power delivered by the wind turbine and photovoltaic module. The proposed control strategy consists of primary and secondary aspects. In the primary layer control, the DC bus voltage is regulated by the GCC. In the secondary layer, the DC bus voltage is maintained by the energy storage device. This ensures reliable power for local loads during grid failures, while power injection to the grid is controlled by an energy management algorithm followed by reference generation of inductor current in the GCC. The proposed control strategy operates in different modes of DC voltage regulation, power injection to the grid and a hybrid operating mode. It provides wide flexible control and ensures the reliable operation of the microgrid. The proposed and conventional techniques are compared for a 15.8 kW DC/AC microgrid system using the MATLAB/Simulink environment. The simulation results demonstrate the transient behaviour of the system in different operating conditions. The proposed control technique is twice as fast in its transient response and produces less oscillation than the conventional system.**

***Index Terms*—Wind energy, photovoltaic energy, DC/AC microgrid, battery energy storage system, coordinated control.**

I. Introduction

The global energy consumption by energy source in 2020 [1] are: oil 31.2%, coal 27.2%, natural gas 24.7%, Hydro 6.9%, nuclear 4.3% and renewables 5.7%. CO_2 emissions from conventional power plants cause global warming. In models of [2] and [3] CO_2 emissions are presented. Fossil-fuel crises, global warming, and climate changes all demand the development of renewable energy resources (RER), which have emerged as a promising solution to address the above issues as elaborated in sustainable development goal 7 (SDG 7) [4]. Among several RER, wind and solar-based systems contribute significant power worldwide [5]. Integration of RER with the utility grid is becoming popular because of cost effectiveness, while worldwide installation of RER has exceeded 750 GW by the end of 2020 [4]–[7]. However, RER power production has irregular characteristics which cause power quality issues. In the literature, a number of maximum power point tracking (MPPT) algorithms are reported, with the most popular including perturbed & observer (P&O) [8], incremental conductance (Inc) [9], and the hill climbing algorithm [10], to enhance power from the photovoltaic (PV) modules. The permanent magnet synchronous generator (PMSG)-based variable speed wind turbine is widely used in industrial application because of advantages of high efficiency, utilizing maximum wind power, and less power fluctuation [11]–[14]. In order to track the maximum power from wind turbines, different types of tracking algorithms have been presented. In [15], a P&O algorithm is discussed. This involves less mathematical computation, but the overall tracking response is slow. Intelligent tracking algorithms such as artificial neural network (ANN)-based and fuzzy MPPT are reported in [16], [17]. These methods have accurate speed tracking capability, but also have high computation complexity and require prior knowledge of the system, and thus are only suitable for large scale plants. In [12],

Received: April 9, 2023
Accepted: November 10, 2023
Published Online: January 1, 2024
Prabhakaran Koothu Kesavan (corresponding author) is with the Renewable Energy Laboratory, the Department of Electrical Engineering, Prince Sultan University, Riyadh, 11586, Saudi Arabia (e-mail: k7prabhakaran@gmail.com).
DOI: 10.23919/PCMP.2023.000272

a tip-speed ratio tracking algorithm is discussed. This involves low computation, has fast speed tracking capability, does not require prior knowledge of the system, and is suitable for medium scale plants.

Solar irradiation and wind velocity are stochastic in nature and power electronics converters have nonlinear characteristics which produce harmonics in current and voltage at the point of common coupling [12], [18]. LCL filters have gained more attention because of superior harmonic reduction capability, low weight and small size. However, the design of LCL involves a lot of mathematical computation. The size of the inverter side inductor and capacitor are dependent on the allowable current ripple, power factor and switching of the converter. Direct power control of a grid connected inverter is reported in [19] and this control algorithm involves phase lock loop (PLL) and an inner current regulator.

One of the major challenges associated with renewable energy systems is the intermittent nature of these resources. This can lead to fluctuations in power generation and grid instability. To address this challenge, microgrid technology has emerged as a potential solution for integrating renewable energy source (RES) into the power grid. Microgrids offer several advantages, including improved reliability, resilience, and flexibility, as well as reduced carbon emissions and energy costs [6]. Additionally, they can operate in grid-connected or islanded modes, allowing them to provide power to critical loads during grid outages or emergencies [20].

There are many papers that have proposed solutions for microgrids in aerospace applications. Reference [21] develops an electricity solution using a DC microgrid based on Moon and Mars using NASA's data. In [22], a general control strategy is proposed to address the power fluctuations at the point of common coupling (PCC) in a solar PV-based grid interactive microgrid system using a hybrid multilevel modular storage system. As interfacing different ratings of solar PV panels to DC microgrid requires an individual power electronic interface and the corresponding control algorithm, a modular multiport converter is introduced in [7] to address this issue where independent MPPT is used to interface with a 380 V DC microgrid through a high-frequency transformer. A similar converter is proposed in [23] in which it handles multiple sources such as PV, wind, and hybrid energy storage in a single converter for DC microgrid application. This converter configuration is controlled in such a way that it handles the frequency fluctuation and achieves power balance in the DC microgrid system. An adaptive DC-link power-based energy management control is proposed in [24] for a grid-connected PV system microgrid application that uses a hybrid energy storage system. This proposed control technique provides a solution for pulse power loading and uncertainty in grid operating conditions. In [11], a predictive control technique is proposed for a full-sized converter applied in PMSG-based wind energy conversation system (WECS). This technique neglects the conventional proportional integral (PI) and PLL to avoid unnecessary complications in the tuning of controllers. An adaptive dynamic reference control technique is proposed for a microgrid system that can handle the non-ideal situation in the system without the need for an accurate system model. A new adaptive fractional frequency control method based on a data-driven algorithm is proposed in [25] for microgrids and low inertia networks to improve the grid frequency stability under different conditions.

The main contributions of this paper are as follows:

1) A modified incremental conductance and tip speed ratio MPPT technique is employed to extract maximum power from the PV array and wind turbine.

2) An energy storage device with a bidirectional DC-DC converter is connected to the common DC bus to provide a constant DC bus voltage during grid failure and changes in wind velocity and solar irradiation.

3) A grid-connected converter with LCL filter is designed to control the injected real power and reactive power compensation to the grid.

4) Generalized power flow management and generation of inductor current reference are implemented to use the maximum renewable energy with minimum utilization of grid power.

5) A two-layer coordinated controller is implemented to provide reliable power to local load and feed excess power to the utility grid.

The paper is organized as follows. In section II, modelling of wind turbine, PMSG, and PV module is presented. System description and the control scheme for wind energy, PV, energy storage conversion system are discussed in Section III. Simulation results for the proposed system are presented in Section IV, and conclusions are given in Section V.

II. Modelling of DC/AC Microgrid

A. Modelling of Wind Turbine

The wind turbine converts the kinetic energy of wind to mechanical power. To study the dynamic response of the wind energy conversion system during variation in wind speed, modelling of wind turbine plays a significant role. The wind turbine model also helps to design the MPPT algorithm.

The mechanical power of a wind turbine can be described as:

$$P_{\mathrm{m}} = \frac{1}{2}\rho A v_{\mathrm{w}}^3 C_{\mathrm{p}} \tag{1}$$

where P_{m} represents the mechanical output power of the wind turbine; ρ represents the air density; A represents the rotor swept area; v_{w} is the wind speed; and C_{p} represents the power coefficient of the wind turbine blades.

The power coefficient of the wind turbine blades can

be defined as:

$$C_{\mathrm{p}}=C_1\left(\frac{C_2}{\lambda_i}-C_3\beta-C_4\right)e^{\frac{-C_5}{\lambda_i}}+C_6\lambda' \tag{2}$$

Where C_1-C_6 represent the coefficients of the wind turbine; β represents the pitch angle; λ' represents the optimal tip speed ratio; and λ_i represents the intermittent tip speed ratio.

The optimal tip-speed ratio is expressed as:

$$\lambda'=\lambda'_{\mathrm{opt}}=\frac{\omega_{\mathrm{r,rated}}R}{v_{\mathrm{w,rated}}} \tag{3}$$

where $\omega_{\mathrm{r,rated}}$ represents the rated speed of the wind turbine; R represents the radius of the wind turbine; and $v_{\mathrm{w,rated}}$ represents the rated wind speed.

The intermittent tip speed ratio is expressed as:

$$\lambda_i=\frac{1}{\lambda'+0.08\beta}-\frac{0.035}{\beta^3+1} \tag{4}$$

The output torque of the wind turbine T_{mech} is expressed as:

$$T_{\mathrm{mech}}=\frac{P_{\mathrm{m}}}{\omega_{\mathrm{r,rated}}} \tag{5}$$

B. Modelling of PMSG

The dynamic model of PMSG is modelled in the *d-q* axis reference frame. The stator voltages in *d-q* axis can be described as:

$$v_{qs}=R_{\mathrm{s}}i_{qs}+\omega_{\mathrm{r}}\psi_{ds}+p\psi_{qs} \tag{6}$$

$$v_{ds}=R_{\mathrm{s}}i_{ds}-\omega_{\mathrm{r}}\psi_{qs}+p\psi_{ds} \tag{7}$$

where v_{ds},v_{qs} represent stator voltage in *d-q* axis; i_{ds},i_{qs} represent stator current in *d-q* axis; R_{s} represents stator resistance; ψ_{ds},ψ_{qs} represent stator flux in *d-q* axis; and ω_{r} represents rotor speed.

$$\psi_{ds}=L_{\mathrm{s}}i_{ds}+\lambda_{\mathrm{m}} \tag{8}$$

$$\psi_{qs}=L_{\mathrm{s}}i_{qs} \tag{9}$$

where L_{s} represents stator inductance and λ_{m} represents rotor flux linkage.

Substituting (8)–(9) into (6)–(7) respectively yields the current in the stator as:

$$\frac{\mathrm{d}}{\mathrm{d}t}\begin{pmatrix}i_{ds}\\ i_{qs}\end{pmatrix}=\begin{pmatrix}-\dfrac{R_{\mathrm{s}}}{L_{\mathrm{s}}} & \omega_r\\ -\omega_{\mathrm{r}} & -\dfrac{R_{\mathrm{s}}}{L_{\mathrm{s}}}\end{pmatrix}\begin{pmatrix}i_{ds}\\ i_{qs}\end{pmatrix}+\begin{pmatrix}\dfrac{1}{L_{\mathrm{s}}} & 0\\ 0 & \dfrac{1}{L_{\mathrm{s}}}\end{pmatrix}\begin{pmatrix}v_{ds}\\ v_{qs}\end{pmatrix}+\begin{pmatrix}0\\ -\dfrac{\lambda_{\mathrm{m}}}{L_{\mathrm{s}}}\end{pmatrix}\omega_{\mathrm{r}} \tag{10}$$

The electromagnetic torque, rotor speed and position are:

$$T_{\mathrm{e}}=\left(\frac{3}{2}\right)\left(\frac{P}{2}\right)(\psi_{ds}i_{qs}-\psi_{ds}i_{ds}) \tag{11}$$

$$T_{\mathrm{e}}-T_{\mathrm{m}}=J\frac{\mathrm{d}\omega_{\mathrm{r}}}{\mathrm{d}t} \tag{12}$$

$$\theta_{\mathrm{r}}=\int\omega_{\mathrm{r}}\mathrm{d}t \tag{13}$$

where $T_{\mathrm{e}},T_{\mathrm{m}}$ represent electromagnetic and mechanical torque; J represents inertia of PMSG; P represents number of poles; and θ_{r} represents rotor position.

C. Mathematical Modelling of Photovoltaic

An equivalent circuit of a PV panel with a single diode model is represented in Fig. 1.

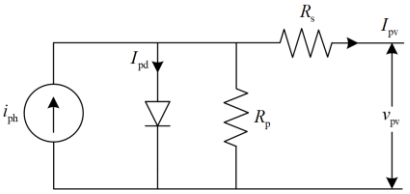

Fig. 1. Equivalent circuit of single diode PV model.

By applying KVL to Fig. 1, the single PV cell current $I_{\mathrm{pv,cell}}$ is computed as:

$$I_{\mathrm{pv,cell}}=I_{\mathrm{ph}}-I_{0,\mathrm{pd}}\left(\mathrm{e}^{\frac{q(V_{\mathrm{pv,cell}}+I_{\mathrm{pv,cell}}\mathrm{R}_{\mathrm{s,pv}})}{akT}}-1\right)-\frac{V_{\mathrm{pv,cell}}+I_{\mathrm{pv,cell}}R_{\mathrm{s,pv}}}{R_{\mathrm{p,pv}}} \tag{14}$$

where I_{ph} represents the PV current; $I_{0,\mathrm{pd}}$ represents the current through the parallel diode; $R_{\mathrm{p,pv}}$ and $R_{\mathrm{s,pv}}$ are the respective parallel and series resistances of PV panel; while $I_{\mathrm{pv,cell}}$ and $V_{\mathrm{pv,cell}}$ represent the output current and voltage of the single PV cell, respectively; k is the Boltzmann constant; q represents the charge of the electron; a represents the curve fitting factor; and T is temperature.

Under uniform irradiation, the PV array current is:

$$I_{\mathrm{pv}}=I_{\mathrm{ph}}N_{\mathrm{pp}}-I_{0,pd}\left(\mathrm{e}^{\frac{q(V_{\mathrm{pv}}+\mathrm{I}_{\mathrm{pv}}\mathrm{R}_{\mathrm{s}}\frac{N_{\mathrm{ss}}}{N_{\mathrm{pp}}})}{akT}}-1\right)-\frac{V_{\mathrm{pv}}+I_{\mathrm{pv}}R_{\mathrm{s}}\dfrac{N_{\mathrm{ss}}}{N_{\mathrm{pp}}}}{R_{\mathrm{p,pv}}\dfrac{N_{\mathrm{ss}}}{N_{\mathrm{pp}}}} \tag{15}$$

where N_{ss} is the number of modules connected in series and N_{pp} is number of modules connected in parallel.

III. Overview of DC/AC Microgrid System

The overall block diagram of the DC/AC microgrid system is shown in Fig. 2. The system is comprised of a permanent magnet synchronous motor (PMSM)-based wind energy conversion system with active rectifier, PV panel with boost converter, energy storage device with bidirectional converter, DC link capacitor, DC load, water pump with variable frequency drive, grid connected converter, LCL filter, and a synchronization relay which will be opened during the islanding mode of operation. In this system, the maximum wind power is extracted by controlling the active three-phase rectifier, the PV maximum power is extracted by controlling the boost converter, and the DC bus voltage is regulated using the bidirectional converter connected to the battery. The grid-connected converter is designed to interface with the utility grid where the inductor current reference for inner loop is generated based on the available active power between the renewable energy source and the utilized local load.

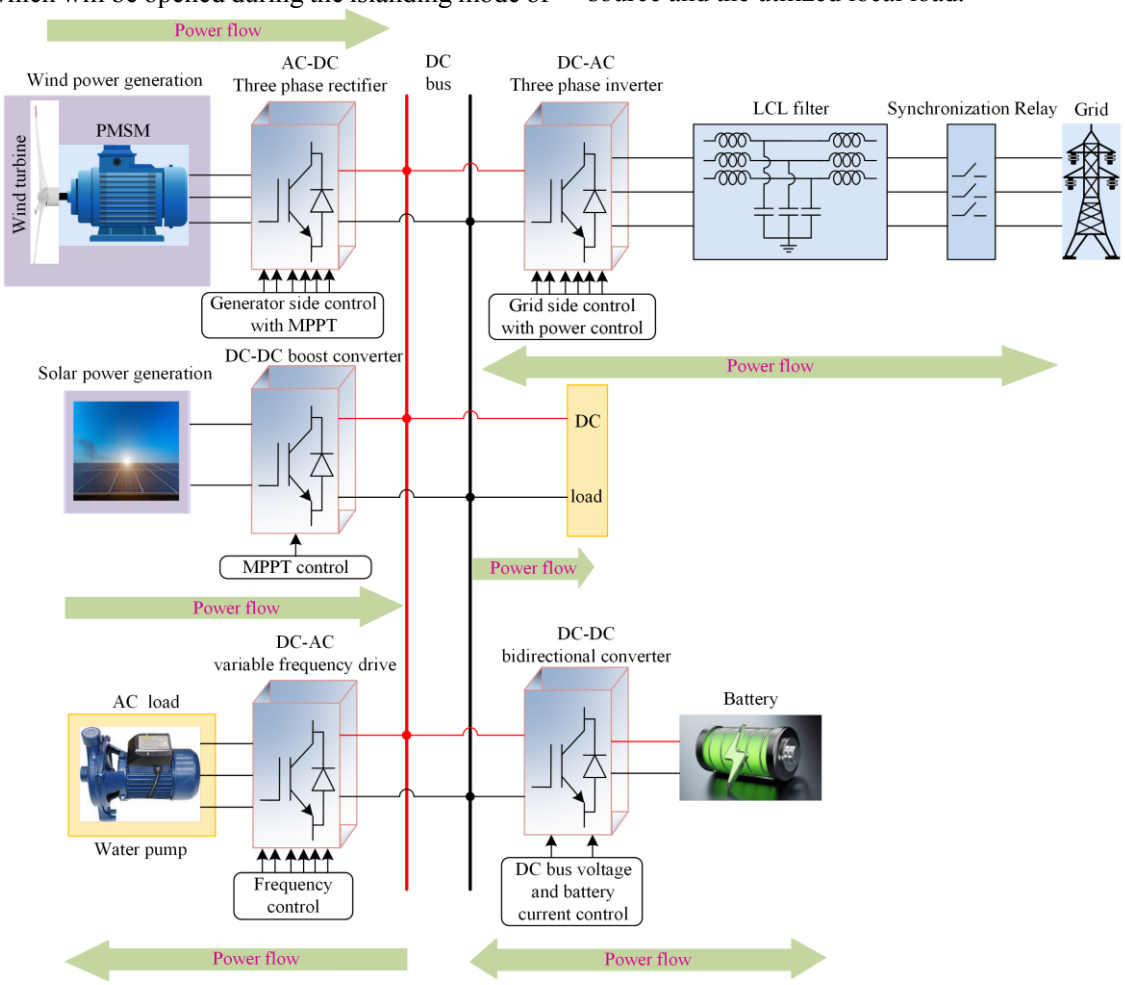

Fig. 2. Simplified overall block diagram of the DC/AC microgrid system.

A. Machine Side Control

The generation of a wind speed reference plays a significant role in the machine side control to extract maximum power from the wind turbine. The control diagram of PMSG connected with active rectifier is shown in Fig. 3. The reference rotor speed is obtained from the optimal tip speed ratio and actual wind speed. The reference speed is:

$$\omega_{\mathrm{m}}^{\mathrm{opt}} = \frac{\lambda'_{\mathrm{opt}} v_{\mathrm{w}}}{R} \tag{16}$$

where $\omega_{\mathrm{m}}^{\mathrm{opt}}$ represents reference rotor speed.

The speed error, obtained from the optimal wind speed and actual speed of PMSM, is regulated as reference electromagnetic torque using the PI speed controller, i.e.:

$$\omega_{\mathrm{r}}^{\mathrm{error}} = \omega_{\mathrm{m}}^{\mathrm{opt}} - \omega_{\mathrm{r}} \tag{17}$$

$$T_{\mathrm{e}}^{*} = k_{\mathrm{p,s}}(\omega_{\mathrm{r}}^{\mathrm{error}}) + k_{\mathrm{i,s}} \int (\omega_{\mathrm{r}}^{\mathrm{error}}) dt \tag{18}$$

where $\omega_{\mathrm{r}}^{\mathrm{error}}$ represents rotor speed error; T_{e}^{*} represents reference electromagnetic torque; $k_{\mathrm{p,s}}$ represents proportional gain of speed controller; and $k_{\mathrm{i,s}}$ represents integral gain of speed controller.

The reference q-axis current (i_{qm}^{*}) is:

$$i_{qm}^{*} = \frac{4T_{\mathrm{e}}^{*}}{3P} \tag{19}$$

The reference voltage is generated using an inner loop current controller to control the machine side converter. The *d-q* axis references are:

$$v_{dm}^{*}=k_{\mathrm{p,mc}}(i_{dm}^{*}-i_{ds})+k_{\mathrm{i,mc}}\int(i_{dm}^{*}-i_{ds})dt-\omega_{\mathrm{e}}L_{\mathrm{s}}i_{qs} \tag{20}$$

$$v_{qm}^{*}=k_{\mathrm{p,mc}}(i_{qm}^{*}-i_{qs})+k_{\mathrm{i,mc}}\int(i_{qm}^{*}-i_{qs})\mathrm{d}t+\omega_{\mathrm{e}}(L_{\mathrm{s}}i_{ds}+\lambda_{\mathrm{m}}) \tag{21}$$

where v_{dm}^{*}, v_{qm}^{*} represent reference machine voltage in *d-q* axis; i_{dm}^{*}, i_{qm}^{*} represent reference stator current in *d-q* axis; $k_{\mathrm{p,mc}}$ represents proportional gain of machine current controller; and $k_{\mathrm{i,mc}}$ represents integral gain of machine current controller.

The *d-q* axis machine voltage references are converted into three-phase machine voltage references using inverse park transformation which are fed as inputs to the pulse width modulation (PWM) generator to generate the switching signal to control the three-phase machine side active rectifier to achieve maximum power from the wind turbine.

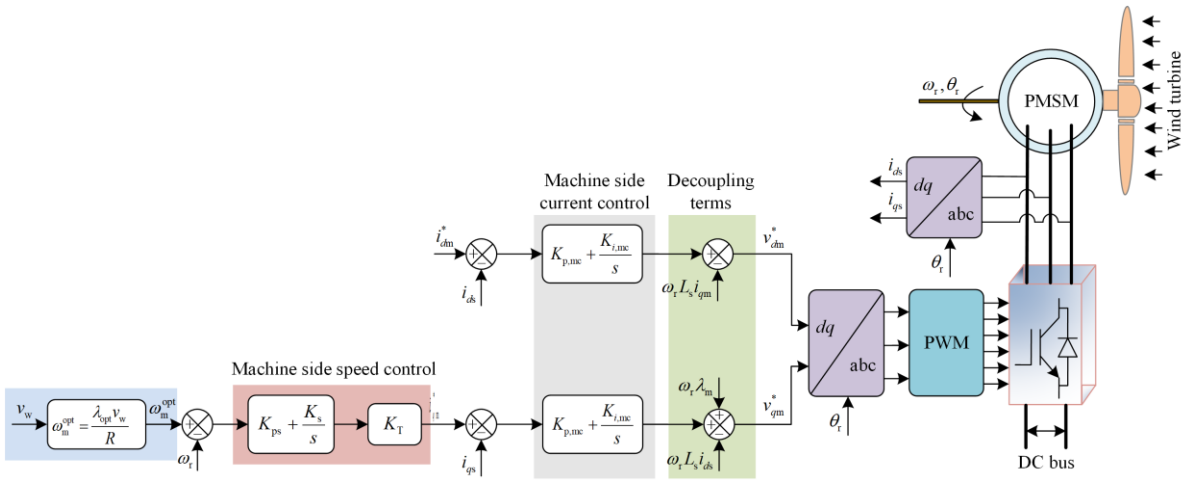

Fig. 3. Control diagram of the PMSM based wind energy conversion system with active rectifier.

B. Control Mechanism of Boost Converter

In this paper, a PV module with boost converter is employed in the microgrid system. The boost converter is controlled by two scenarios as shown in Fig. 4. In the first scenario, a modified incremental conductance MPPT algorithm is implemented to extract the maximum power from the PV module as shown in Fig. 5. In this case, the DC bus voltage is maintained by the battery with the bidirectional converter. However, in the case where the battery state of charge is less than 60 %, if the battery continues to support to DC bus voltage, this can cause a reduced lifetime of the battery. To prevent battery degradation, the second scenario is implemented. The MPPT algorithm is deactivated when the state of charge of the battery is less than 60 % and the DC bus voltage regulation loop is activated. Thereby, the PV panel supports the maintenance of the DC bus voltage and delivers the power.

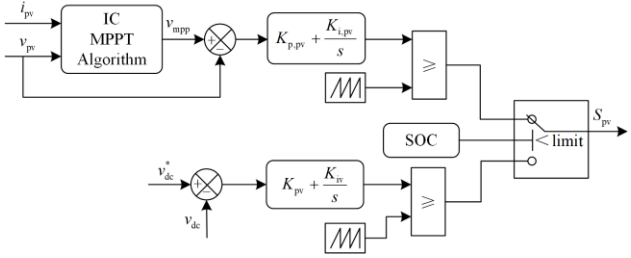

Fig. 4. Control diagram of the boost converter connect with solar panel.

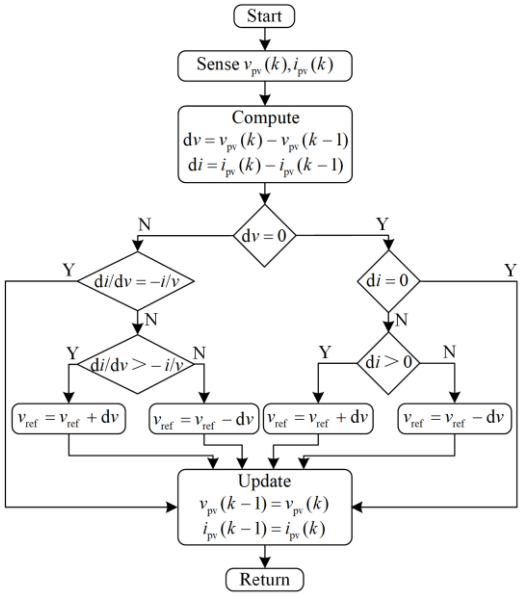

Fig. 5. Flow chat of modified incremental conductance maximum power point algorithm.

C. Control Mechanism of Bidirectional Converter

The schematic of the energy storage device control logic consists of two loops as shown in Fig. 6. The outer loop regulates the DC bus voltage, and the inner loop regulates battery current. In the outer loop the DC bus voltage error is computed and passed through the PI voltage controller to generate the reference battery current. The battery current error signal is then calculated

and passed through the PI current controller to generate the reference duty cycle. The gating signal of the bidirectional converter is then generated (for charging mode S_{b1} is activated and for discharging mode S_{b2} is activated).

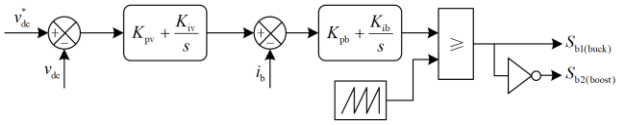

Fig. 6. Control diagram of the bidirectional converter connect with battery.

D. Power Flow Management Algorithm for DC/AC Microgrid

The flow chart of the reference active power, reactive power and synchronization angle (θ_g) generation is shown in Fig. 7. The power flow management algorithm provides two modes of operation: grid-connected mode and islanded mode. In grid-connected mode, the θ_g is computed by the synchronous reference frame (SRF)-PLL where grid voltages are considered as input to the SRF-PLL. The grid-connected converter operates in three different operating conditions. Case 1: Power generated from the renewable energy source (P_{gen}) is equal to the power required of the local load (P_{local}) and the injected real power to the grid is thus set to zero. Case 2: P_{gen} is greater than the P_{local} requirement, and the real power injection to the grid is set to positive (i.e., real power injection is the computed difference between power from the renewable energy and local load). Case 3: P_{gen} is less than P_{local} the requirement, and the real power injection to the grid is set to negative so that the excess power required to the local load is met by the utility grid. Islanded mode is realised by the absence of the grid connection, and the grid-connected converter is disconnected from the DC bus. Case 1: P_{gen} is greater than P_{local} requirement which is considered as safe operation. Case 2: P_{gen} is less than P_{local} requirement which is considered as critical operation and non-essential loads are disconnected.

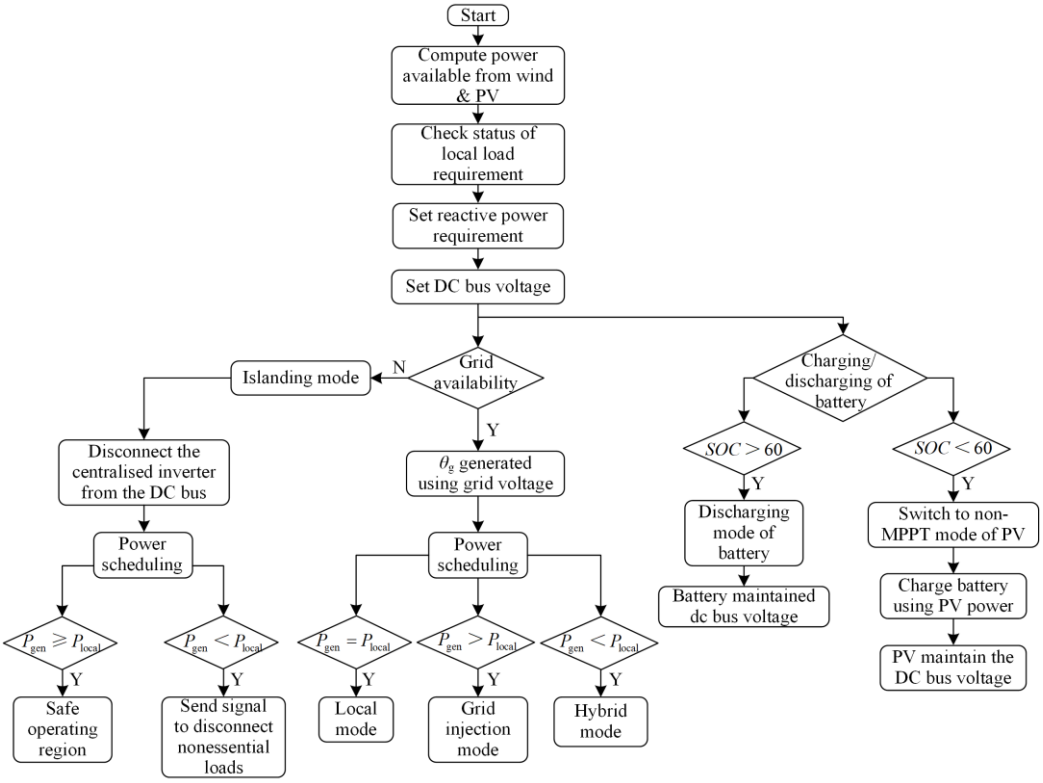

Fig. 7. Flow chart for the energy management of DC/AC microgrid.

E. Grid side control

The grid side control technique is shown in Fig. 8 and is comprised of two layers. Both control layers require θ_g which is computed using the SRF-PLL to ensure proper synchronization between converter output and grid voltages. The first layer involves DC bus voltage regulation and inductor current regulation, and the second layer involves the reference generation of inductor current based on the available power from renewable energy and regulates the inductor current.

The available real power from the renewable energy source is:

$$P_{gen} = P_{wind} + P_{solar} + P_{battery} \tag{22}$$

where $P_{wind}, P_{solar}, P_{battery}$ represent power generated by wind, solar and power stored in battery.

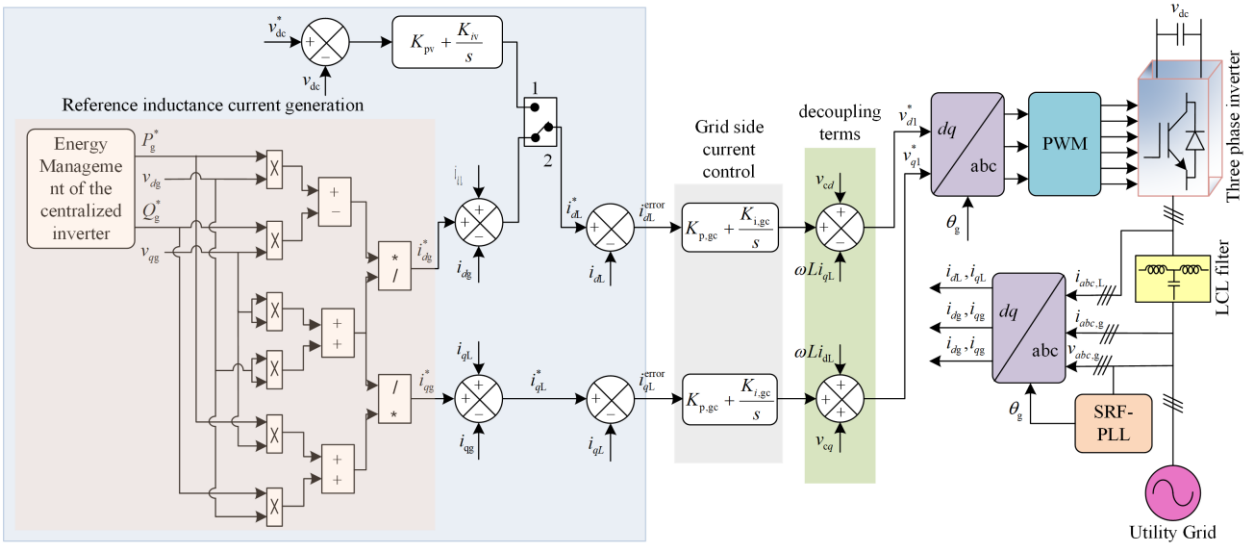

Fig. 8. Control diagram of the centralized inverter connected with utility grid.

The power used by the local load P_{local} is:

$$P_{\text{local}} = P_{\text{dc (dc load)}} + P_{\text{ac (pump load)}} \tag{23}$$

where $P_{\text{dc (dc load)}}$ and $P_{\text{ac (pump load)}}$ represent DC load and pump load.

The reference active power injection through the centralized inverter is:

$$P_{\text{g}}^{*} = P_{\text{gen}} - P_{\text{local}} \tag{24}$$

where P_{g}^{*} represents reference active power.

The *d-q* axis grid current references are:

$$i_{dg}^{*} = \frac{v_{dg}P_{\text{g}}^{*} - v_{qg}Q_{\text{g}}^{*}}{v_{dg}^{2} + v_{qg}^{2}} \tag{25}$$

$$i_{qg}^{*} = \frac{v_{qg}P_{\text{g}}^{*} + v_{dg}Q_{\text{g}}^{*}}{v_{dg}^{2} + v_{qg}^{2}} \tag{26}$$

where i_{dg}^{*}, i_{qg}^{*} represent reference grid current in *d-q* axis; $P_{\text{g}}^{*}, Q_{\text{g}}^{*}$ represent active and reactive of grid power; and v_{dg}, v_{qg} represent grid voltage in *d-q* axis.

The reference *d-q* axis inductor currents ensure that the maximum real power is transferred to the grid. The *d-q* axis reference inductor currents are generated using instantaneous *d-q* axis references, actual grid currents and actual inductor currents, and are expressed as:

$$i_{d\text{L}}^{*} = i_{dg}^{*} + i_{\text{cd}} = i_{dg}^{*} + (i_{d\text{L}} - i_{dg}) \tag{27}$$

$$i_{q\text{L}}^{*} = i_{qg}^{*} + i_{\text{cg}} = i_{qg}^{*} + (i_{q\text{L}} - i_{qg}) \tag{28}$$

where $i_{d\text{L}}^{*}, i_{q\text{L}}^{*}$ represent reference inductor current in *d-q* axis; i_{dg}, i_{qg} represent grid current in *d-q* axis; $i_{d\text{L}}, i_{q\text{L}}$ represent filter inductor current in *d-q* axis; and $i_{d\text{C}}, i_{q\text{C}}$ represents filter capacitor current in *d-q* axis.

In the grid side control, the inner loop current controller regulates inductor current errors to generate reference voltages. These are used to control the centralized inverter to ensure reliable and stable operation, as:

$$v_{d\text{L}}^{*} = k_{\text{p,gc}}(i_{d\text{L}}^{*} - i_{d\text{L}}) + k_{\text{i,gc}}\int (i_{d\text{L}}^{*} - i_{d\text{L}})\text{d}t - \omega L_{\text{s}} i_{q\text{L}} + v_{cd} \tag{29}$$

$$v_{q\text{L}}^{*} = k_{\text{p,gc}}(i_{q\text{L}}^{*} - i_{q\text{L}}) + k_{\text{i,gc}}\int (i_{q\text{L}}^{*} - i_{q\text{L}})\text{d}t + \omega L_{\text{s}} i_{d\text{L}} + v_{cq} \tag{30}$$

where $v_{d\text{L}}^{*}, v_{q\text{L}}^{*}$ represent reference inductive voltage in *d-q* axis; $k_{\text{p,gc}}$ represents proportional gain of grid current controller; and $k_{\text{i,gc}}$ represents integral gain of grid current controller.

The *d-q* axis inductive voltage references are converted into three-phase voltage references using inverse park transformation and are fed as inputs to the PWM generator to generate switching signals for the three-phase grid-connected inverter.

IV. Results and Discussion

Simulation studies are carried out for the DC/AC hybrid microgrid under different wind speeds, irradiation, and load conditions to demonstrate the efficacy of the proposed control strategy. The parameters of the system are presented in Tables I–V. The system consists of a 9 kW PMSM based wind turbine, 4.36 kW PV generations where four solar panels are connected in series and 2 parallel strings are connected to formulate a module, a 2.2 kVA lithium-ion battery energy storage where two 72 V batteries are connected in series, a 7 kW DC load and a 2.2 kW PMSM based water pump. The simulation study is carried out in the MATLAB/Simulink environment using the proposed and conventional controllers [19] in different scenarios:1. variations in wind speed and irradiation; and 2. variation in the load.

TABLE I
WIND TURBINE AND PMMS PARAMETERS DETAILS

Parameters	Values
Rated power	9 kW
Stator resistance	0.0485 Ω
Stator inductance	0.395 mH
Permanent magnet flux linkage	0.1192 Wb
Inertia	0.0085 kg·m^2
Pole pair	4
Optimal tip speed ratio	8.1
Radius of wind turbine	1.2 m
Proportional gain of speed controller (K_{ps})	0.2
Integral gain of speed controller (K_{is})	0.9
Proportional gain of machine current controller ($K_{p,mc}$)	1.1
Integral gain of machine current controller ($K_{i,mc}$)	150

TABLE II
SOLAR PANEL PARAMETERS DETAILS

Parameters	Values
Open circuit voltage	49.75 V
Voltage at maximum power point	41.8 V
Short circuit current	13.93 A
Current at maximum power point	13.04 A
Power at maximum power point	545 W
Proportional gain of MPPT controller ($K_{p,mp}$)	0.05
Integral gain of MPPT controller ($K_{i,mp}$)	0.001

TABLE III
BATTERY PARAMETERS DETAILS

Parameters	Values
Nominal voltage	72 V
Nominal current	30 Ah
Proportional gain of DC link voltage controller ($K_{p,vb}$)	0.5
Integral gain of DC link voltage controller ($K_{i,vb}$)	4.8
Proportional gain of battery current controller ($K_{p,cb}$)	0.02
Integral gain of battery current controller ($K_{i,cb}$)	3

TABLE IV
WATER PUMP PMMS PARAMETERS DETAILS

Parameters	Values
Rated power	2.2 kW
Stator resistance	0.5 Ω
Stator inductance	4.33 mH
Permanent magnet flux linkage	0.572 Wb
Inertia	3.1×10^{-4} kg·m^2
Pole pair	2
Proportional gain of pump speed controller ($K_{p,ps}$)	0.02
Integral gain of pump speed controller ($K_{i,ps}$)	1.2
Proportional gain of pump current controller ($K_{p,pc}$)	50
Integral gain of pump current controller ($K_{i,pc}$)	8000

TABLE V
THREE PHASE INVERTER DESIGN PARAMETERS DETAILS

Parameters	Values
Input DC voltage	380 V
Phase-phase voltage	220 V
Rated output power	15 kVA
Switching frequency	10 kHz
Filter inductor (L_1)	0.95 mH
Filter inductor (L_2)	1.35 mH
Filter capacitor (C)	50 μF
Proportional gain of grid current controller ($K_{p,gc}$)	1.2
Integral gain of grid current controller ($K_{i,gc}$)	480

A. Performance of the system during variations of wind speed and irradiation conditions.

In this case, simulation results are given in Fig. 9 to show the dynamic response of power injection to the grid during variations in wind speed and irradiation conditions. Fig. 9(a) shows the power delivered by the wind turbine and generator speed during change in wind velocity (initial wind velocity is 8 m/s and then is varied to 13 m/s at 2 s, and 10 m/s at 4 s, respectively). Based on the MPPT technique, the machine side converter effectively varies the operating point of the wind turbine speed and corresponding maximum power delivered as shown in Fig. 9(a), i.e., 2.63 kW at 67 rad/s, 8.46 kW at 127 rad/s, and 4.77 kW at 87 rad/s. Fig. 9(b) shows the

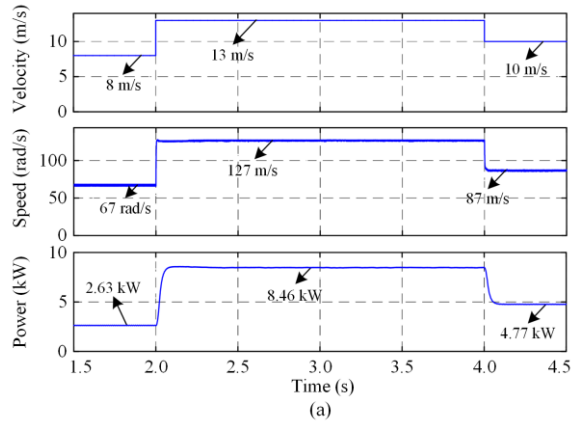

(a)

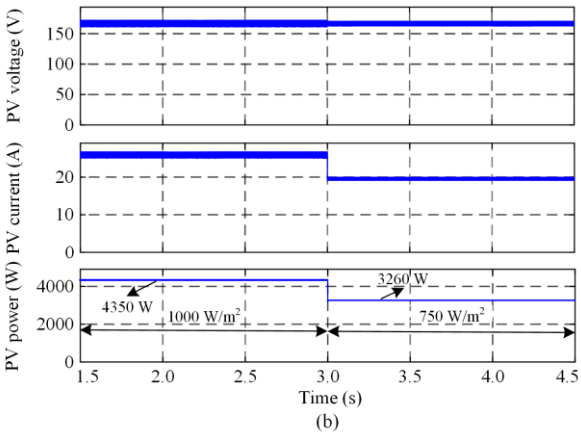

(b)

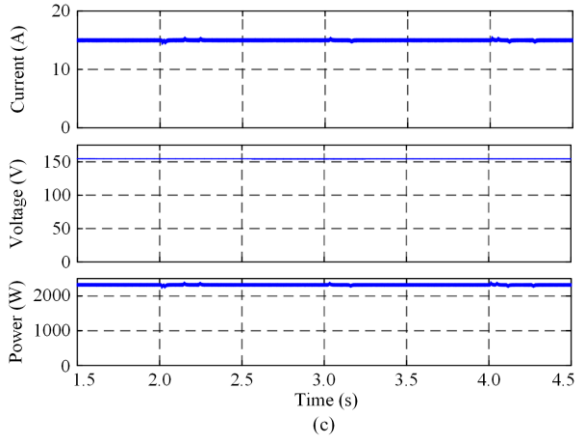

(c)

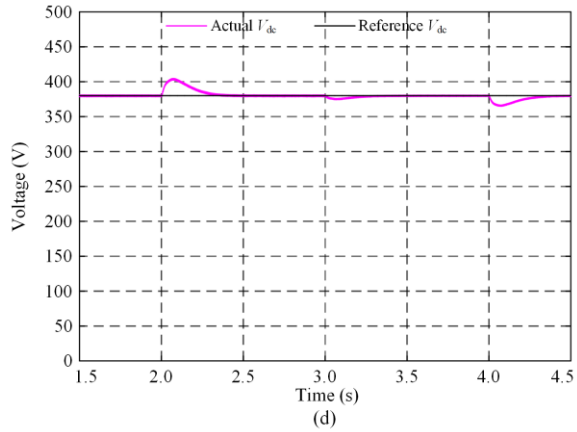

Fig. 9. Dynamic performance of the system during variations of wind speed and irradiation conditions at power generation side. (a) wind power generation. (b) solar power generation. (c) battery power. (d) DC bus voltage.

PV voltage, current and power corresponding to the maximum power point for the solar module. Initially, solar power is generated at 1000 W/m^2, while at 3 s the irradiation is changed from 1000 W/m^2 to 750 W/m^2. Corresponding to the change in irradiation, maximum power extraction using the modified IC is 4350 W and 3260 W at 1000 W/m^2 and 750 W/m^2, respectively as shown in Fig. 9(b). The battery operates in the discharge mode, and it is observed from Fig. 9(c) that power delivered by the battery is around 2.2 kW. Fig. 9(d) shows that the DC bus voltage is maintained at a constant value of 380 V.

When the 7 kW constant DC load is connected, the corresponding results are shown in Fig. 10. It is seen from Fig. 10(a) that, in the presence of perturbations in the wind velocity and solar irradiation, the proposed coordinated control algorithm maintains a constant DC voltage of 380 V and load current of around 18.42 A. The proposed control technique computes the availability of real power based on power generated by the RES whereas real power has to be set manually in the existing control technique. The *d-q* axis grid currents, three-phase grid currents, power injection to the grid, and grid voltage response are shown in Figs. 10 (b)–(f) during changes in wind speed and irradiation for the proposed and conventional control techniques. It is clearly seen that, with the proposed control technique the *d-q* axis grid currents, three-phase grid currents and power injection to the grid have faster transient response, quicker setting time and less oscillation than the conventional control technique [19] during dynamic changes in the system. It can also be seen that reactive power injection to the grid is maintained at zero whereas the conventional technique has more transient overshoots. In addition, the proposed controller has smooth response during uncertainty in wind speed, change in irradiation while also eliminating power quality issues as per IEEE Std. 519-2014.

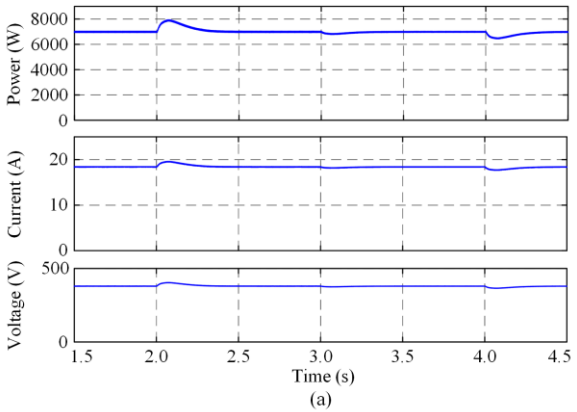

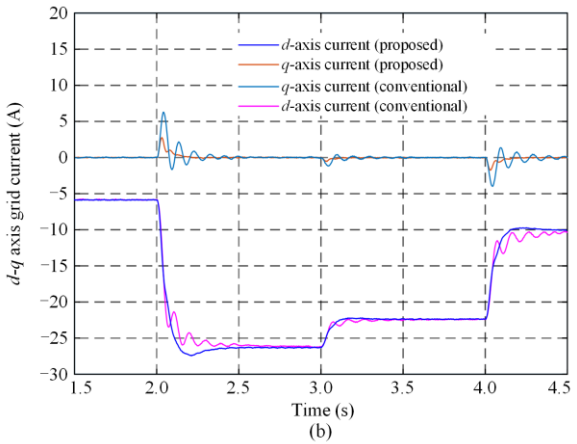

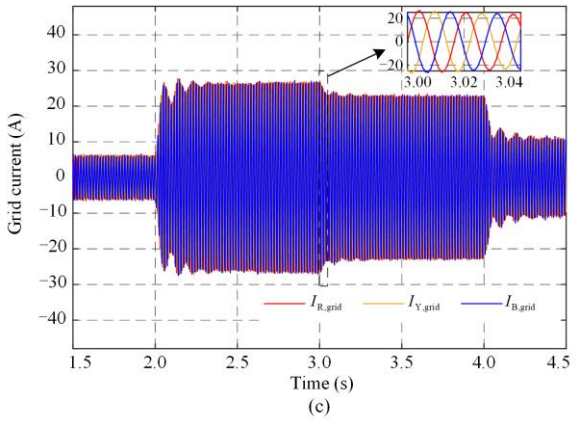

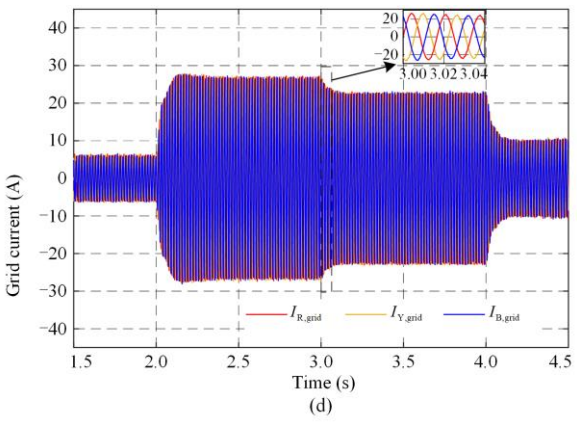

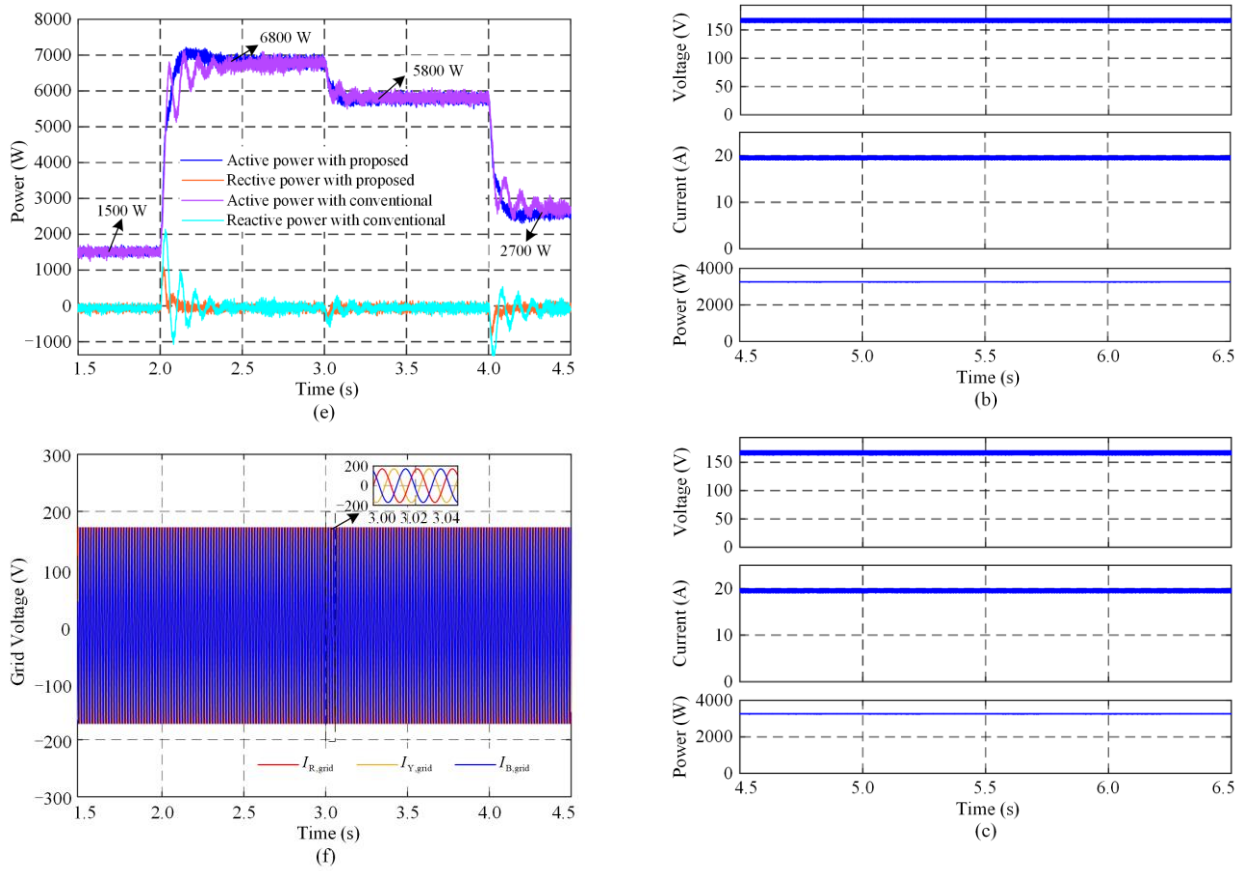

Fig. 10. Dynamic performance of the system during variations of wind speed and irradiation conditions at DC load and grid side. (a) DC load. (b) *d-q* axis grid current. (c) grid current with conventional control. (d) grid current with proposed control. (e) power injection to grid. (f) grid voltage.

B. Dynamic Behaviour of the System During Load Change

The dynamic behaviour of the system during load variation is validated and the results are presented in Figs. 11 and 12. In this case, irradiation is maintained at 750 W/m^2, wind speed is varied from 10 m/s to 8 m/s at 5 s as shown in Fig. 11(a), and the PMSM-based water pump is ramped up from standstill to rated speed from 5.5 s to 6.2 s, as shown in Fig. 11(e). In addition, to

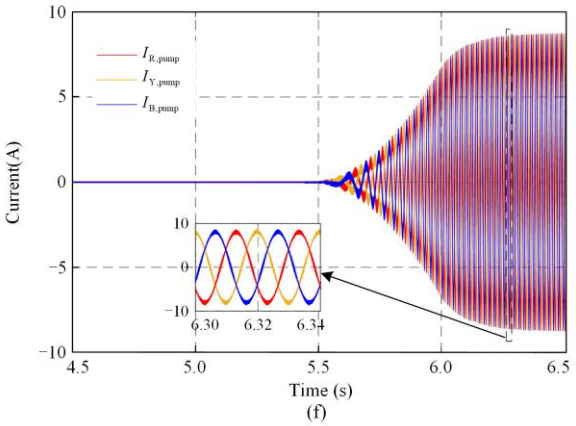

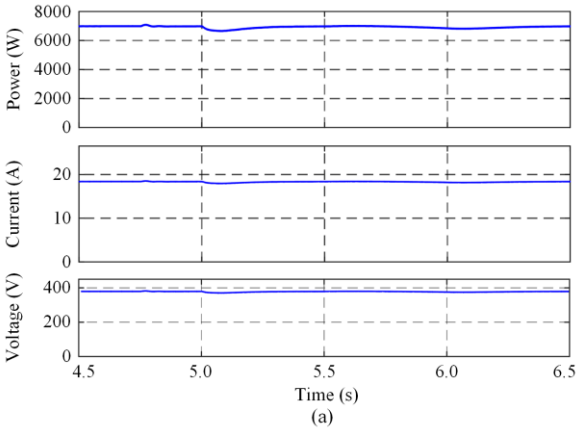

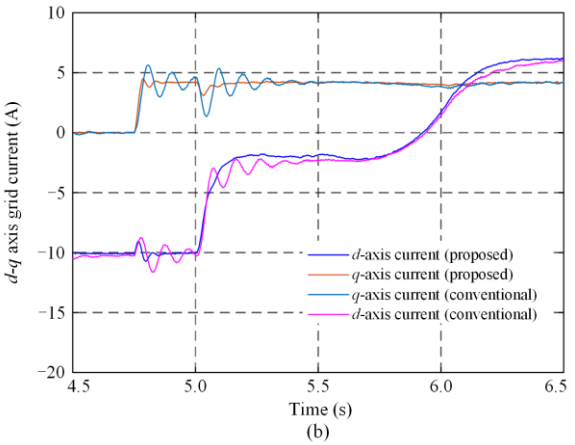

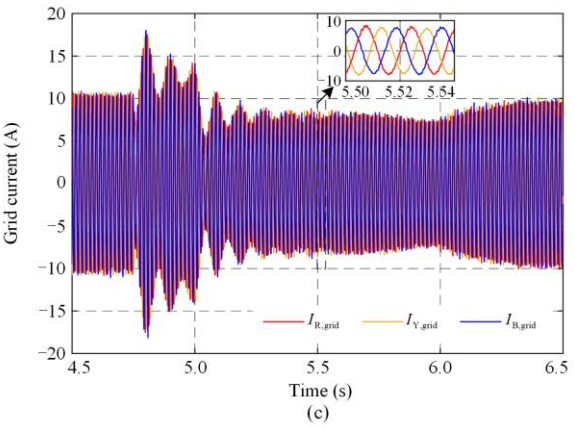

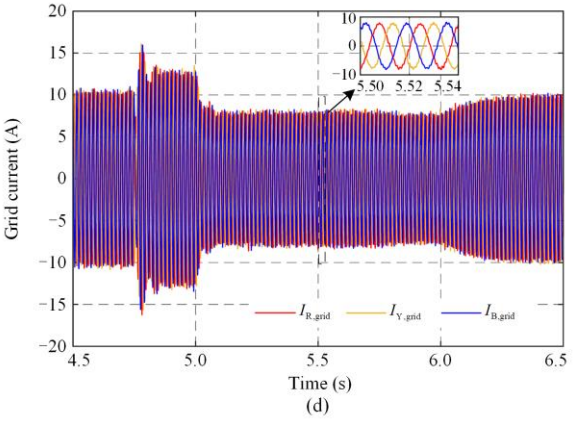

Fig. 11. Dynamic behaviour of the system during load change at power generation side and water pump. (a) wind power generation. (b) solar power generation. (c) battery power. (d) DC bus voltage. (e) speed of the water pump. (f) current of the water pump.

validate the controller performance, a constant 7 kW DC load is applied for the entire region and at 4.75 s, 2000 var is injected to grid as shown in Fig. 12.

From Figs. 11 and 12, The following observations can be made:

1) Initially the total power produced by the wind turbine, solar panel and battery is 10.16 kW, while power consumed by the DC load is 7 kW and power injected to the grid is 2.6 kW, Therefore the efficiency of the overall system is around 94.5 %.

2) During change in wind speed, the power generated by the RES is around 8 kW and the total power used by the local load and injected to the grid is around 7.5 kW. The efficiency of the system is around 93.75 %.

3) From 5.5 s to 6.2 s, the 2.2 kW pump load gradually ramps up from stand still to rated speed. Consequently, power demand required by the local load is raised to 9.2 kW but the power produced by the RES is around 8 kW, the extra required power is thus consumed from the grid.

4) From Figs. 12 (b)–(e), it is clearly seen that, with the proposed control technique the *d*-*q* axis grid currents, three-phase grid currents and power injection to the gird have faster transient response, quicker settling time and less oscillation than those with the conventional controller during dynamic changes in the system.

5) At 4.75 s, when a 2000 var reactive power is injected to grid, the response with the proposed controller is much smoother than that of the conventional control technique which has more transient overshoots and has a longer settling time.

6) In addition, with the proposed controller the overall system has smooth response during a change in load condition while also eliminating power quality issues as per IEEE Std 519-2014.

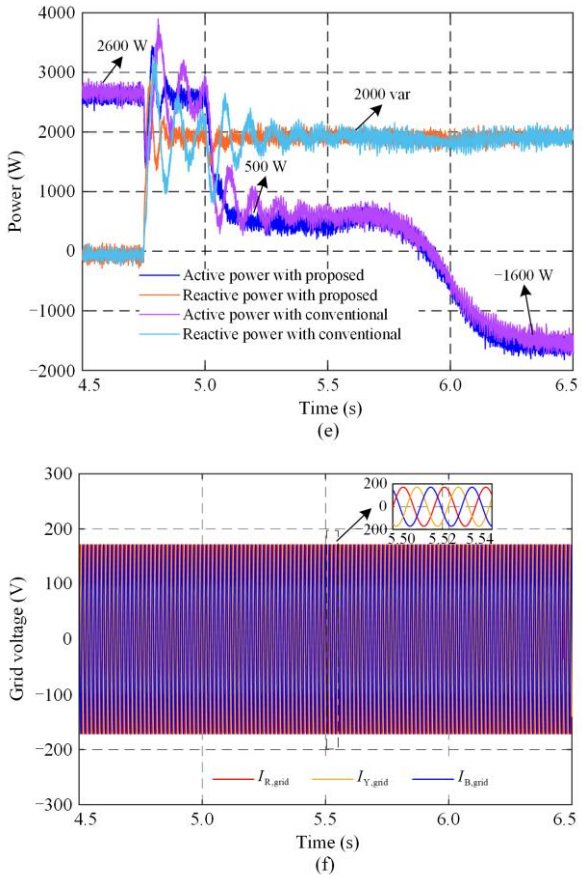

Fig. 12. Dynamic behaviour of the system during load change at grid side. (a) DC load. (b) *d-q* axis grid current. (c) grid current with conventional control. (d) grid current with proposed control. (e) power injection to grid. (f) grid voltage.

Table VI compares the performance of the proposed and conventional controllers [19] for the 15.8 kW DC/AC microgrid. It is inferred that the proposed controller has superior performance to the conventional controller. The proposed controller is capable of mitigating grid current, and real and reactive power to grid. It has smoother transient response, quicker settling time and less overshoot in the grid current, real and reactive power than the conventional one.

TABLE VI
PERFORMANCE EVALUATION OF PROPOSED CONTROLLER WITH THE CONVENTIONAL CONTROLLER

	Proposed controller	Conventional controller
Overshoot of real power	10 %	23.35 %
Settling time of real power	0.2 s	0.4 s
Overshoot of three phase current	7.2 %	18.5 %
Settling time of three phase current	0.1 s	0.3 s
Effect of parametric uncertainty	No	Yes
Ripple mitigation at grid	P_g^* , Q_g^* , I_g	P_g^* , Q_g^*

V. CONCLUSION

In this paper, a multilayer coordinated control technique and power flow management for a DC/AC microgrid system is presented. The DC/AC microgrid consists of a PMSG-based wind turbine, photovoltaic module, energy storage device, grid connected converter, DC load, and water pump. In the primary layer, a DC voltage regulator is employed in the grid connected converter to maintain the DC bus voltage at a constant level. The secondary layer control is implemented to share the power to the local load and grid during variations of wind velocity and solar irradiation. In the secondary layer control, the DC bus voltage is maintained by controlling the energy storage device to ensure constant DC bus voltage during grid failure. Furthermore, power injection to the grid is controlled by a power flow management algorithm and inductor current reference in the grid connected converter. In the case that the state of charge of the energy storage is less than 60 %, the MPPT mode of the PV module is deactivated, and the DC bus voltage regulation mode is activated for the PV with boost converter. Further, an energy storage device is configured to charge mode and power sharing is scheduled accordingly. The simulation results are obtained for the DC/AC microgrid with the proposed coordinated control technique and with the conventional technique of the grid-connected converter. The simulation results demonstrate that the proposed coordinated algorithm eliminates the power scheduling limitation and enhances the transient behaviour of the overall system. In addition, the results highlight that the proposed control strategy reduces oscillations in grid power and has smoother changes in the grid current than the conventional controller. It is also important to note that the proposed techniques can be used with various hybrid systems, i.e., integration of hydropower plant and solar plant to the utility grid, and integration of solar, electric vehicle, super capacitor into utility grid.

ACKNOWLEDGEMENT

The authors would like to acknowledge the support of Renewable Energy Lab, Prince Sultan University, Saudi Arabia.

AUTHORS' CONTRIBUTIONS

Prabhakaran Koothu Kesavan: original draft preparation, conceptualization, methodology, software, data curation, formal analysis. Umashankar Subramaniam: supervision, reviewing, and editing. Dhafer Jaber Almakhles: supervision, reviewing, and editing. Sivakumar Selvam: data collection. All authors read and approved the final manuscript.

FUNDING

This work is supported by Prince Sultan University, Riyadh, Saudi Arabia, under research grant SEED-2022-CE-95.

AVAILABILITY OF DATA AND MATERIALS

Not applicable.

DECLARATIONS

Competing interests: The authors declare that they have no known competing financial interests or personal relationships that could have appeared to influence the work reported in this paper.

AUTHORS' INFORMATION

Prabhakaran Koothu Kesavan received the B.E. degree in electrical and electronics engineering and the M. E. degree in power electronics and drives from Anna University, Chennai, India, in 2011 and 2013, respectively, and the Ph.D. degree in electrical and electronics engineering from the National Institute of Technology Karnataka, Surathkal, India, in 2019. He was a Postdoctoral Fellow with the Hydropower Simulation Laboratory, Department of Water Resource Development and Management, Indian Institute of Technology Roorkee, Roorkee, India, from September 2019 to December 2021. Later, he worked as a senior lead engineer-electrical system, Aerostrovilos Energy Pvt. Ltd associated with Indian Institute of Technology Madras, India. Currently, he is working as a postdoctoral researcher with the renewable energy, Prince Sultan University, Saudi Arabia. His research interests include nonlinear control, control of power converters, industrial drives, power electronics applications in renewable energy systems and power conditioning.

Umashankar Subramaniam received the B.E. degree in Electrical and Electronics Engineering from Govt. College of Technology, Coimbatore, in the year 2001, and M. Tech. in Power Electronics and PhD in Electrical Engg., (Specialization in Energy) from VIT University, Vellore, in the years 2004 and 2013, respectively. Currently, he is working as an associate professor in the College of Engineering and a Researcher in the Renewable Energy Lab at Prince Sultan University. Formerly, he worked as an associate professor in School of Electrical Engineering, VIT University, Vellore. He worked as assistant professor-senior, senior R&D engineer, and senior application engineer in the power electronics, renewable energy, and electrical drives field for over 20 years. He has published/presented more than 250 papers in national and international journals/conferences and holds two U.S patents. He has also co-authored/co-edited 10 books/chapters and 10 technical articles on power electronics applications in renewable energy and allied areas. His current areas of research activities include power electronics applications in wind and solar energy, electric vehicle and charging infrastructure, smart grid, and power quality.

Dhafer Jaber Almakhles received the B.E. degree in electrical engineering from the King Fahd University of Petroleum and Minerals, Dhahran, Saudi Arabia, in 2006, and the master's (Hons.) and Ph.D. degrees from The University of Auckland, New Zealand, in 2011 and 2016, respectively. Since 2016, he has been with Prince Sultan University, Saudi Arabia, where he is currently the chairperson of the Communications and Networks Engineering Department and the Director of the Science and Technology Unit. He is also the leader of the renewable energy research team and the laboratory at Prince Sultan University. His research interests include the hardware implementation of control theory, signal processing, networked control systems, and sliding mode.

Sivakumar Selvam received the B.E. degree in electrical and electronics engineering and the M.E. degree specialized in power electronics and drives from Anna University, Chennai, in 2013 and 2015, respectively. He worked as an assistant professor with the Saranathan College of Engineering, India, from 2015 to 2020. He is currently working as lecturer with the Electrical Engineering, Renewable Energy Laboratory, Prince Sultan University, Saudi Arabia. He has authored more than ten articles in international journals and conferences proceedings. His research interests include grid interfaced solar PV systems, multilevel inverters, DC–DC converters for microgrid applications, and digital control of power converters.

REFERENCES

[1] T. Ahmad, and D. Zhang, "A critical review of comparative global historical energy consumption and future demand: The story told so far," *Energy Reports*, vol. 6, pp. 1973-1991, Nov. 2020.

[2] G. Aydin, "The modeling of coal-related CO_2 emissions and projections into future planning," *Energy Sources, Part A: Recovery, Utilization, and Environmental Effects*, vol. 36, no. 2, pp.191-201, Jan. 2014.

[3] I. Karakurt, G. Aydin, and S. Kaya *et al*., "Forecasting of Turkey's coal consumption using grey prediction technique," in *Proceedings of 24th International Mining Congress of Turkey,* Antalya, Turkey, Apr. 2015, pp.77-82.

[4] K. Shulla, W. L. Filho, and S. Lardjane *et al*., "Sustainable development education in the context of the 2030 Agenda for sustainable development," *International Journal of Sustainable Development and World Ecology*, vol. 27, no. 5, pp. 458-468, Jul. 2020.

[5] A. G. Olabi and M. A. Abdelkareem. (2022, Apr.). "Renewable energy and climate change," *Renewable and Sustainable Energy Reviews*. [Online]. Available: https://doi.org/10.1016/j.rser.2022.112111

[6] T. Adefarati, R. C. Bansal, and J. John Justo, "Techno-economic analysis of a PV-wind-battery-diesel standalone power system in a remote area," *The Journal of Engineering*, no. 13, pp. 740-744, 2017.

[7] A. Vettuparambil, K. Chatterjee, and B. G. Fernandes, "A modular multiport converter to integrate multiple solar photo-voltaic (PV) modules with a battery storage system and a DC microgrid," *IEEE Transactions on Industrial Electronics,* vol. 69, no. 5, pp. 4869-4878, May, 2022.

[8] A. K. Abdelsalam, A. M. Massoud, and S. Ahmed *et al*., "High-performance adaptive perturb and observe MPPT technique for photovoltaic-based microgrids," *IEEE Transactions on power electronics,* vol. 26, no. 4, pp.1010-1021, Apr. 2011.

[9] F. Liu, S. Duan, and F. Liu *et al*., "A variable step size INC MPPT method for PV systems," *IEEE Transactions on industrial electronics,* vol. 55, no. 7, pp. 2622-2628, Jul. 2008.

[10] B. N. Alajmi, K. H. Ahmed, and S. J. Finney *et al*., "Fuzzy-logic-control approach of a modified hill-climbing method for maximum power point in microgrid standalone photovoltaic system," *IEEE Transactions on Power Electronics*, vol. 26, no. 4, pp. 1022-1030, Apr. 2011.

[11] K. Koiwa, Y. Li, and K. Z. Liu *et al*., "Full converter control for variable-speed wind turbines without integral controller or PLL," *IEEE Transactions on Industrial Electronics*, vol. 67, no. 11, pp. 9418-9428, Nov. 2020.

[12] M. K. K. Prince, M. T. Arif, and A. Gargoom *et al*., "Modeling, parameter measurement, and control of PMSG-based grid-connected wind energy conversion system," *Journal of Modern Power Systems and Clean Energy*, vol. 9, no. 5, pp. 1054-1065, Sept. 2021.

[13] H. Shutari, T. Ibrahim, and N. B. M. Nor *et al*., "Development of a novel efficient maximum power extraction technique for grid-tied VSWT system," *IEEE Access*, vol. 10, pp. 101922-101935, 2022.

[14] M. E. Haque, M. Negnevitsky and K. M. Muttaqi, "A novel control strategy for a variable-speed wind turbine with a permanent-magnet synchronous generator," *IEEE Transactions on Industry Applications*, vol. 46, no. 1, pp. 331-339, Jan.- Feb. 2010.

[15] W. Qiao, X. Yang and X. Gong, "Wind speed and rotor position sensorless control for direct-drive PMG wind turbines," *IEEE Transactions on Industry Applications*, vol. 48, no. 1, pp. 3-11, Jan.- Feb. 2012.

[16] A. M. Eltamaly and H. M. Farh, "Maximum power extraction from wind energy system based on fuzzy logic control," *Electric Power System Research.,* vol. 97, pp. 144-150, Apr. 2013.

[17] F. Jaramillo-Lopez, G. Kenne and F. Lamnabhi-Lagarrigue, "A novel online training neural network-based algorithm for wind speed estimation and adaptive control of PMSG wind turbine system for maximum power extraction," *Renew. Energy*, vol. 86, pp. 38-48, Feb. 2016.

[18] A. Reznik, M. G. Simões, and A. Al-Durra *et al*., "LCL filter design and performance analysis for grid-interconnected systems," *IEEE Transactions on Industry Applications*, vol. 50, no. 2, pp. 1225-1232, Mar.-Apr. 2014.

[19] Y. Gui, X. Wang and F. Blaabjerg, "Vector current control derived from direct power control for grid-connected inverters," *IEEE Transactions on Power Electronics*, vol. 34, no. 9, pp. 9224-9235, Sept. 2019.

[20] S. Fazal, M. E. Haque, and M. T. Arif *et al*., "Grid integration impacts and control strategies for renewable based microgrid," *Sustainable Energy Technologies and Assessments,* vol. 56, Mar. 2023.

[21] B. Saude, N. LaSart, and J. Blair *et al*., "Microgrid-based wind and solar power generation on moon and mars," *IEEE Transactions on Smart Grid*, vol. 14, no. 2, pp. 1329-1332, Mar. 2023.

[22] M. B. Hossain, M. R. Islam, and K. M. Muttaqi, *et al*., "A compensation strategy for mitigating intermittencies within a PV powered microgrid using a hybrid multilevel energy storage system," *IEEE Transactions on Industry Applications*, vol. 59, no. 4, pp. 5074-5086, Jul.-Aug. 2023.

[23] B. R. Ravada, N. R. Tummuru and B. N. L. Ande, "Photovoltaic-wind and hybrid energy storage integrated multi-source converter configuration for DC microgrid applications," *IEEE Transactions on Sustainable Energy*, vol. 12, no. 1, pp. 83-91, Jan. 2021.

[24] M. K. Behera and L. C. Saikia, "A novel resilient control of grid-integrated solar PV-hybrid energy storage microgrid for power smoothing and pulse power load accommodation," *IEEE Transactions on Power Electronics*, vol. 38, no. 3, pp. 3965-3980, Mar. 2023.

[25] M. V. Kazemi, S. J. Sadati and S. A. Gholamian, "Adaptive frequency control of microgrid based on fractional order control and a data-driven control with stability analysis," *IEEE Transactions on Smart Grid*, vol. 13, no. 1, pp. 381-392, Jan. 2022.